International Journal of Advanced Biological and Biomedical Research
Available online at http:www.ijabbr.com
Volume 9, Issue 1 (2021) pp. 28-47 **DOI**: 10.22034/ijabbr.2021.44618

Original Article

A 3-Dimentional Framework for Studying the Effects of Structural and Physical Properties of the Renal Outer Medulla on Urine Concentrating Mechanism

Maryam Saadatmand[1*], Mohammad Said Saidi[2], Salman Sohrabi[2], Mohamad Hossein Banazadeh[2], Saeed Sadeghi Lafmejani[2], Hamid Hamed[1], Bahar Firoozabadi[2]

[1]Department of Chemical and Petroleum Engineering, Sharif University of Technology, Tehran, Iran
[2]Department of Mechanical Engineering, Sharif University of Technology, Tehran, Iran

*Corresponding Author E-mail: m.saadatmand@sharif.edu

Received: 20 June 2020, Revised: 30 August 2020, Accepted: 31 August 2020

ABSTRACT

Background: Many theories and mathematical simulations have been proposed concerning urine concentrating mechanism (UCM). Due to significant effect of the tubule and vessel architecture in concentrating mechanism, the numerical analysis of UCM through a 3-Dimensional structure might be the answer to find a better consistency between the experimental and theoretical results.

Methods: In this paper we have investigated the effects of structural characteristics of the tubules and vessels on the urine concentrating mechanism in the outer medulla (OM) by developing a simple three-dimensional mathematical model. This model is a framework to attain a converged numerical solution for the momentum and species transport equations along with their stiff and coupled boundary conditions based on standard expressions for trans-tubular solutes and water transports on tubule's membrane.

Results: The model structure and the number of the involved tubules have been assumed to be as simple as possible. The effects of slip boundary condition on membrane, Darcy permeability and solute's diffusivity of the intermediate media on UCM have been studied. It has been shown that this approach can simply simulate preferential interactions and tubule's confinement by radial diffusion coefficients.

Conclusions: All in all, the feasibility of the idea of completely 3-D modeling by employing the concept of diffusion coefficient and Darcy permeability has been explored and validated.

Key words: 3-Dimensional modeling, Interstitium physical properties, Structural characteristics

1. Introduction

The ability to maintain the osmolality balance between blood plasma and the outlet urine as one the fascinating features of kidney makes it one of the most complicated organs of human body [1]. Urine concentrating mechanism (UCM), as the main process in regulating water excretion, has been widely studied by both experimental and theoretical

approaches [2]. Since some physiological characteristics of UCM can be easily explained, developing novel mathematical methods seems crucial to gain a better understanding of this process [3, 4].

Longitudinal section of kidney has three main layers with different characteristics: cortex, outer medulla and inner medulla. In spite of an isosmotic fluid flow with respect to arterial blood within the cortex, a cortico-papillary gradient of osmolality within the medulla is thought to be the most reliable explanation for the higher osmolality in outlet urine. There are various theories, which have tried to explain this phenomenon. According to the countercurrent multiplication mechanism, active reabsorption of solute from ascending tubules is the reason for the osmotic pressure difference between descending and ascending limbs of the loop of Henle [5, 6]. This mechanism is able to explain osmotic gradient in outer medulla but steepest gradient in inner medulla could not be explained by this theory, because long ascending tubules in this region have no active transepithelial transport [7-10].

According to Stephenson [11] and Kokko and Rector [12], the interstitium has much higher urea concentration than NaCl concentration and the fluid in Henle's loop has much higher NaCl concentration than urea concentration. This hypothesis, known as the passive mechanism, is critically dependent on specific loop of Henle permeabilities to NaCl and urea. Although the validation of mathematical models based on the passive mechanisms with experimental models on urine osmolality showed their ability to predict, but the inconsistency between aforementioned mathematical models' results and experimentally measured urine osmolality has actuated researchers to study the effects of anatomic complexity.

Wexler and colleagues [13, 14] investigated the effect of 3-D architecture of renal medulla on urine concentrating mechanism. They attributed weighted factors (value between 0-1) to each tubule and vessel to describe the distances and also the amount of solute exchange between them. In their model, there is no intermediate environment like medullary interstitium for solute exchange. Therefore, each tubule, according to the weighted factor, directly interacts with nearer vessels. The need for more acute models of three-dimensional structure of tubules and vasa recta in inner and outer medulla has led many physiological and mathematical researchers to reconstruct computer-based three-dimensional architecture of the renal medulla and investigate its role in urine concentrating mechanism [15, 16].

The more precise studies in this area have been done by Layton's group [17, 18]. To simulate the 3-D organization of tubules and vessels in the renal medulla, they introduced a region approach based on explanatory description of physiologist investigations [19-21]. In this approach, there are some distinct regions in every medullary level in which different tubules and vasa recta are distributed between them by a specific order. Spaces between tubules and vasa recta are considered as interstitial space, interstitial cells and capillaries. Tubules and vessels exchange solutes and water with surrounding environment and not directly to one another. It should be noted that each region has constant solute concentrations but these concentrations differ from one another between regions. In their early study, [22] divided the outer medulla cross section in two regions, but they upgraded it into four regions in their following work [17] in order to have a more realistic model. Their investigation in 2011 [23] which also took into account the inner medulla, is the most complete and thorough 1-D mathematical simulation of

renal which has been presented so far up to our knowledge.

The diameter and length of nephron tubules are in the order of micrometer and millimeter, respectively, and because of this significant dimensional difference, previous researchers used a system of one-dimensional equations to describe this tissue mathematically [3, 23-28]. However, this assumption for medulla environment, exterior to the tubules and vasa recta, appears to be inconsistent with anatomical and physiological studies. As mentioned before, a region approach was used to compensate the effect of concentration gradients by regionalization. However, again for each region the concentration gradients are considered unidirectional in the cortico-medullary axis direction. Therefore, as attested by other researchers, regionalization cannot thoroughly compensate the effect of three-dimensional species transport [22, 29]. Based on the complexity of tubule's architecture revealed in anatomic and physiological studies. It is recently proposed [3, 4] a 3-D model to more accurately simulate the UCM. They introduced a detailed functional unit based on specific configuration of vascular bundles which is much closer to the living renal tissue. The numerical results showed agreement with tissue slice experiments.

Since the nephron has a number of distinct tubules with different membrane transport properties, the steady state model for the UCM consists of a high order system of coupled and nonlinear ODEs. Due to high values of hydraulic and solute permeability of some renal tubules, these equations are usually stiff. Therefore the solving of these equations in 3-D seems very critical as the complexity of the physical and architectural properties of the outer medulla cannot be thoroughly simulated with one dimensional models [4, 22].

The principle goal of this study was to describe a simple 3-D numerical model of the urine concentrating mechanism as a framework to study how the structural properties of outer medulla might affect operational indexes of UCM including mass transfer and hydrodynamic regimes. In the following sections, a central core model of outer medulla has been represented and then its formulation, parameters and boundary conditions have been described and discussed in details. It should be noted that in this simulation, the main focus was on converging and finding the numerical solution for the 3-D, stiff and coupled set of equations in order to investigate the effect of structural properties on UCM. In addition to the base case profiles in which 3-D and 1-D numerical solutions have been compared, the solute gradients in a cross section of medullary interstitium have been studied for its different physical properties.

2. Material and Methods

In this study, the central core (CC) formulation which was proposed in previous [11], has been used. As discussed before, the purpose of this study is just simulating UCM in a model structure as simple as possible; therefore, the significant importance of vasa recta has been overlooked. An important fact about vasa recta shown by Layton and Layton [17] is that vasa recta tend to track concentrations of interstitial fluid. Another fact is that both ascending vasa recta (AVRs) and descending vasa recta (DVRs) membranes have sufficiently high water and solute permeability. Considering these findings, computational costs and 3-D structural complications, using central core assumption and simplifying vasa recta by an intermediate porous medium, have been seemingly convincing enough at the moment. Therefore, all constituents of medulla other than tubules, *e.g.* ascending and descending vasa recta, interstitial cells,

interstitial spaces and capillaries have been represented as one porous intermediate compartment.

One short-looped nephron, including the descending Henle's loop (DHL), ascending Henle's loop (AHL) and Collecting duct (CD) in the outer medulla (OM) and Distal tubule (DT) in cortex, has been considered as a filtration unit. It should be also noted that this simulation has been just considered as a framework that more detailed mathematical simulations has been reported before [30] .

The schematic of the discussed model structure is demonstrated in Figure 1, in which the loop of Henle and CD may exchange with each other through the outer medullary interstitium (OMI). The DHL, AHL and CD are oriented along the cortico-medullary axis, which extends from x=0 at the cortico-medullary boundary to x = L_{OM} at the OM-IM boundary. DT connects AHL to CD and is located in the cortical interstitium (CI) in which fluid is essentially isosmotic to arterial blood. According to literature, although many organic and inorganic compounds are involved in UCM, sodium, chloride, potassium and urea are the most influential solutes. In this simulation Na^+ (as a representative of both NaCl and KCl), urea and water are assumed to be involved in the mathematical modeling [4, 31, 32].

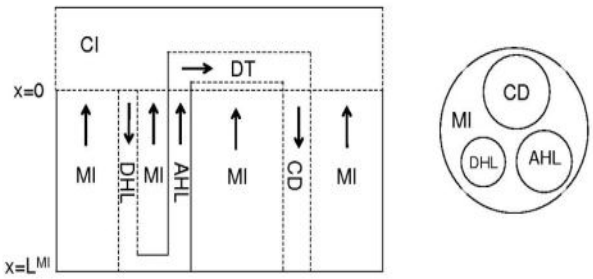

Figure 1. Schematic of central core model.Left: Tubules and surrounding interstitium, CI, Cortex interstitium; MI, Medullary interstitium; DHL, Descending Henle's loop; AHL, Ascending Henle's loop; DT, Distal tubule; CD, Collecting duct; Dashed lines: water permeable boundaries; Arrows: steady-state flow directions. Right: Medulla cross-section showing connectivity between MI and other tubules

2.1. Model equations

Conservation of mass (Eq. 1), momentum equations (Eq. 2) and two species transport equations (Eq. 3) are the main equations which might be simultaneously solved in their 3-D form [4, 32-34].

Continuity equation:

$$\nabla . V = 0 \qquad (1)$$

Momentum transport equation (in 3 directions):

$$\rho V . \nabla (V) = -\nabla P + \mu (\nabla^2 V) \qquad (2)$$

Finally, two concentration equations (for each k) represented the species transport are as follows:

$$V . \nabla C_k = D_k (\nabla^2 C_k) \quad , k = 1,2 \qquad (3)$$

Where the subscripts 1 and 2 are for Na^+ and urea, respectively. In these equations the terms V, P, C_k and D_k are the 3D velocity vector, fluid pressure, concentration of solute k and diffusion coefficient of solute k in the tubular or interstitial fluid respectively. The ρ and μ are fluid density and fluid viscosity, respectively.

The aforementioned momentum equations are valid for the interior regions

of each tubule while the outer medullary interstitium is modeled as a porous compartment in which the momentum equations for interstitial fluid could be rewritten as:

$$\mu V = -\kappa \nabla . P \qquad (4)$$

Where κ is Darcy permeability. As discussed in our previous study, solute's diffusivity in interstitial fluid can be used to perfectly create and simulate the concept of radial concentration gradients [4]. It should be noted that in our previous study, OMI has been assumed not to be porous, but in current study we have modeled the OMI as a porous compartment to find its effect on the UCM.

2.2. Boundary conditions

At the entrance of DHL, a steady mass flow rate with parabolic profile and constant Na^+ and urea concentrations have been set (Table 1). Moreover, pressure outlet boundary condition has been used at the end of collecting duct (CD), as shown in Table 1. Likewise, appropriate boundary conditions for outer medullary interstitium region should also be determined for the 3-D structure. The model structure has been assumed to be representative of a renal filtration unit and due to the symmetry, the outer wall of medulla has been considered to be impermeable to solutes and interstitial fluid. It is showed [33] that the effect of interstitial and solutes flow rate from the inner to the outer medulla on the result's profiles is negligible. Thus, based on this notion and also for simplicity, this model has been assumed to be closed at x = L^{OM}, *i.e.* there is no convective flow at x = L^{OM} into the medullary interstitium.

Table 1. Boundary conditions [33]

Variable	$DHL\ @\ x = 0$	$CD(@\ x = L^{CD}$
$F_v\left(\frac{nl}{min}\right)$	10.0	-
$C_{Na^+}(mM)$	140.0	-
$C_{urea}(mM)$	5.0	-
$P(mmHg)$	0	6.4

In OMI, the flow direction has been assumed to be toward the cortical interstitium because of the dominant number of ascending vasa recta. Furthermore, due to the abundance of blood vessels in the cortex, solutes quickly get carried away as they reach the cortico-medullary boundary. Thus, zero diffusive boundary condition has been used for solutes at the cortico-medullary boundary [20].

Additionally, solutes and fluid fluxes on the tubule' membrane are important boundary conditions to specify the interactions between tubules and their surrounding interstitium. To this purpose, water flux has been formulated by both pressure gradient and osmotic driven forces where solute flux has been determined by the solvent convection as well as a combination of passive and active transport in which passive transtubular transport has been described by Kedem and Katchalsky model [35], while active transtubular transport has followed Michaelis-Menten kinetics. Therefore, transtubular water flux, J_v^i, and solute flux, J_k^i, can be written as:

$$J_v^i = h_v^i[\sum_k R_s T\left(C_k^{MI} - C_k^i\right)\sigma_k^i \phi_{osm,k} + P^i - P^{MI}] \quad (i = DHL, AHL, CD) \qquad (5)$$

$$J_v^i = h_v^i[\sum_k R_g T\left(C_k^{CI} - C_k^i\right)\sigma_k^i \phi_{osm,k} + P^i - P^{CI}] \quad (i = DT) \qquad (6)$$

$$J_k^i = J_v^i(1-\sigma_k^i)\left(\frac{C_k^i+C_k^{MI}}{2}\right) + h_k^i(C_k^i - C_k^{MI}) + \frac{V_{max,k}^i C_k^i}{K_{M,k}^i + C_k^i} \quad (i = DHL, AHL, CD) \quad (7)$$

$$J_k^i = J_v^i(1-\sigma_k^i)\left(\frac{C_k^i+C_k^{CI}}{2}\right) + h_k^i(C_k^i - C_k^{CI}) + \frac{V_{max,k}^i C_k^i}{K_{M,k}^i + C_k^i} \quad (i = DT) \quad (8)$$

Where for *i*-th tubule and solute *k*, h_v^i is hydraulic permeability, h_k^i is passive permeability, σ_k^i is Staverman reflection coefficient of the membrane, C_k^i is the concentration and P^i is the pressure. The last term in Equations 7 and 8 stands for the active transport of solute k in *i*-th tubule in which $V_{max,k}^i$ is the maximum rate of transport and $K_{M,k}^i$ is Michaelis constant. In the above equations, R_g and T are universal gas constant and absolute temperature, respectively. Furthermore, $\phi_{osm,k}$ is the osmotic coefficient of solute *k*. Also, it should be noted that in Equations 5 to 8, the positive flux direction for both solutes and fluid fluxes are assumed to be into the medullary interstitium. The cortical interstitium constants are presented in Table 2. Likewise, model parameters, along with their units and the physical constants are listed in Tables 3, 4, respectively.

Table 2. Cortical interstitium properties [33]

Variable	Value
$C_{Na^+}^{CI}(mM)$	140.0
$C_{urea}^{CI}(mM)$	5.0
$P^{CI}(mmHg)$	0.0

2.3. Solving method

The numerical solution of the transport equations in the five domains in our structure including DHL, AHL, DT, CD and OMI is not a dilemma since mass and momentum equations (Eq. 1 and Eq. 2) are independent of solute concentrations. Besides, the velocity dependence of transport equations (Eq. 3) does not complicate the solving procedure. However, most of the complexity within numerical solution is due to solutes and water fluxes on tubular membrane since membrane's water flux (Eq. 5 and Eq. 6) is a function of both solute concentrations and pressure. Additionally, solute fluxes (Eq. 7 and Eq. 8) are also a function of solute concentrations as well as the water flux. Therefore, membrane's fluxes are coupled with Eq. 1 to Eq. 3 which will subsequently cause some complication with stability of 3-D numerical modeling.

In order to mathematically solve these coupled equations in our model, an unstructured grid has been generated. As shown in the Figure 2, prism cell shapes have been used for meshing the inner regions of tubules as well as the outer medullary interstitium. It has been depicted that the cells become bigger when closer to the outer wall of OMI, since the cells have to be smaller just in the tubule's neighboring regions.

Rayan was used to solve the flow field and species transport equations. This native code is an arbitrary polyhedral grid co-located incompressible finite volume solver. More explanation on the features of Rayan can be found in [36]. Moreover, some of the other features of Rayan like new search algorithms and open boundary condition are also reported in open literature [37, 38]. Rayan can solve steady and transient flows along with scalar transport. It is

also capable of handling dynamic meshes using arbitrary Eulerian-Lagrangian approach.

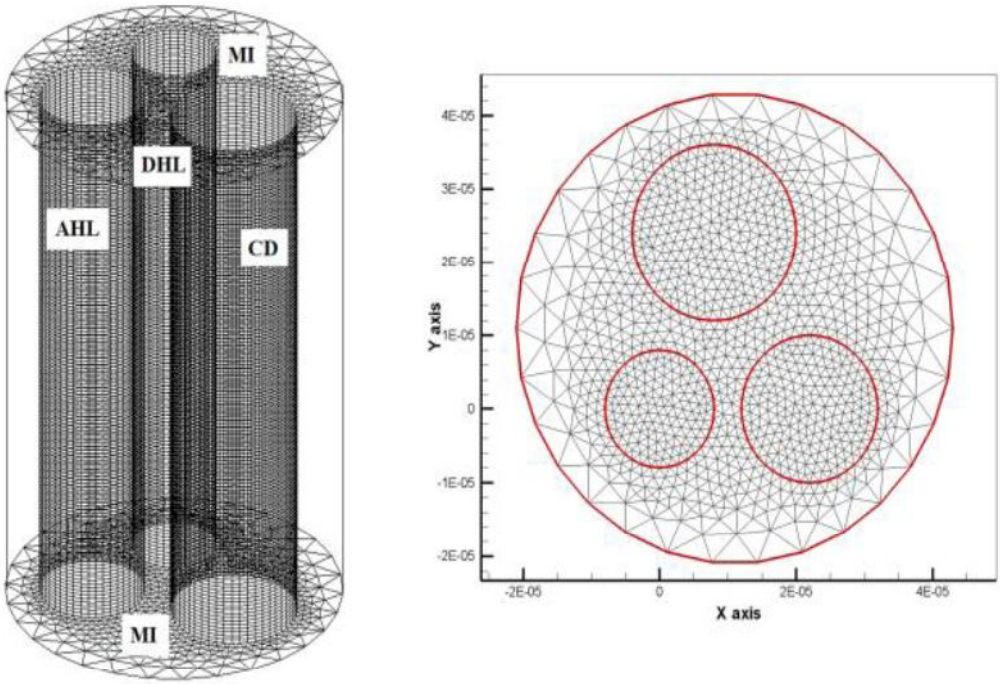

Figure 2. Schematic of 3-D unstructured grid generated for outer medullary model structure

The general description of the numerical method which has been used for solving mass, momentum and species transport equations (Eq. 1 to Eq. 3) in this study, has been discussed in detail in previous research when our native code, Rayan, has been introduced [38]. It should be mentioned that the particular formulations for membrane's fluid and solutes fluxes has been introduced to the main code as boundary conditions, meaning that for simultaneously solving zones together, the face of every marginal prism cell on each side of tubule's membrane should be linked to that of at the other side in order that it would be able to read the concentrations and pressure data at either side to compute fluxes. The direction of these fluxes has been assumed to be normal to the surface of marginal faces whereas no slip assumption for hydrodynamic boundary condition has been considered to be in the tangential direction of the membrane's surface at both sides.

Instability and solution divergence happened because of a rapid concentration change at each of tubule's membrane side, using an under relaxation factor for the membrane fluxes in the model. This relaxation factor has just transferred fraction of the flux's differences computed in the current iteration to the next. Thus, it has been contrived in the code so that, most importantly, the solute concentrations of the marginal cells have changed gradually and caused smoother convergence of the numerical solution ultimately, an appropriate value for this factor has been treated by trial and error in order to achieve minimum computational costs.

Table 3. Base-case Parameters [33, 39]

Parameter	DT	AHL	DHL	MI	CD
$h_v(10^{-12}\left(\frac{m}{Pa.s}\right))$	1.5	0.0	17.1	-	5.0
$h_{Na^+}(10^{-7}m/s)$	0.1	1.61	1.61	-	0.4
$h_{urea}(10^{-7}m/s)$	0.0	0.86	1.5	-	0.0
$V_{max,Na^+}(10^{-5}(\frac{mol}{m^2s}))$	0.93	6.1	0.0	-	0.0
$V_{max,urea}(10^{-5}(\frac{mol}{m^2s}))$	0.0	0.0	0.0	-	0.0
$K_{max,Na^+}(10^{-5}(\frac{mol}{m^3}))$	0.075	0.15	0.0	-	0.0
$K_{max,urea}(10^{-5}(\frac{mol}{m^3}))$	0.075	0.15	0.0	-	0.0
σ_{Na^+}	1.0	1.0	0.96	-	1.0
σ_{urea}	1.0	1.0	0.96	-	1.0
ϕ_{osm,Na^+}	1.84	1.84	1.84	-	1.84
$\phi_{osm,urea}$	1.0	1.0	1.0	-	1.0
$Radius(10^{-6}m)$	12.0	10.0	8.0	32.0	12.0
$Length(10^{-2}m)$	1.0	0.4	0.4	0.4	0.4
$D_{Na^+}(10^{-9}m^2/s)$	1.5	1.5	1.5	1.5	1.5
$D_{urea}(10^{-9}m^2/s)$	1.38	1.38	1.38	1.38	1.38

Table 4. Physical constants [33, 39]

Physical variable	Value
$\boldsymbol{T_k}$	310.15
$\mu(\boldsymbol{\frac{kg}{m.s}})$	0.0006915
$\boldsymbol{\rho\left(\frac{kg}{m^3}\right)}$	993.33
$\boldsymbol{R_g(\frac{J}{mol.K})}$	8.314

3. Results and discussion

In this section, the results from three-dimensional modeling of fluid and solute transport in a nephron are discussed. Previously defined base-case parameters and appropriate boundary conditions, guarantee steady-state solutions for water and solute transport in the renal outer medulla.

Additionally, for comparison purposes, a native code developed before by authors for 1-D modeling solute and water transport in the renal outer medulla, has been used [38]. Its boundary conditions and parameters values were equal to those mentioned in Table 1-4. Furthermore, the orthogonal collocation method was used as the solution method.

Figures 3-6 depict the results of 3-D and 1-D simulations in which their Na^+ and Urea concentration, pressure and velocity data nearly have the same distribution and are in a well agreement. However, there are some differences between the profiles of 3-D and 1-D results along the nephron's length. It could be said that in 1-D model, OMI solute concentrations at every medullary depth is considered uniform. In other word, radial solute permeability in interstitial fluid is infinitive because there is no resistance for transport in radial direction. On the contrary, in 3-D base case simulation, the OMI radial diffusion

coefficient has been assumed to have the same values as tubular fluid. Furthermore, as explained earlier, due to simplicity of base case's model structure, the Na^+ and urea concentration distributions are fairly reliable. Accordingly, they cannot be compared with experimental data or results from previous work [17].

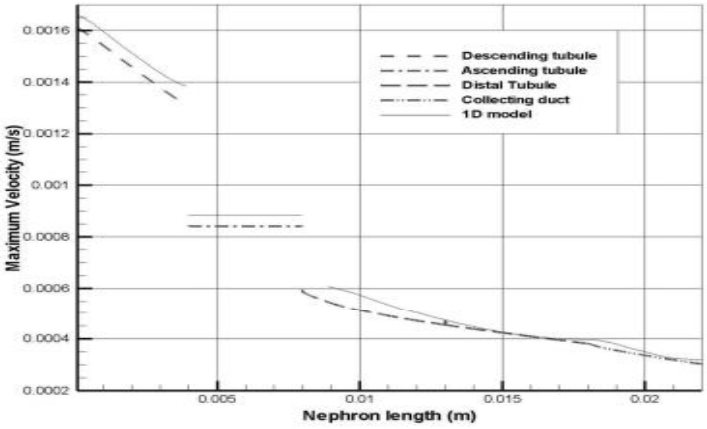

Figure 3. Maximum fluid velocity distribution along nephron from entrance of DHL to the end of CD in 3-D and 1-D model, the discontinuities in velocity figures are due changes in tubule's radius

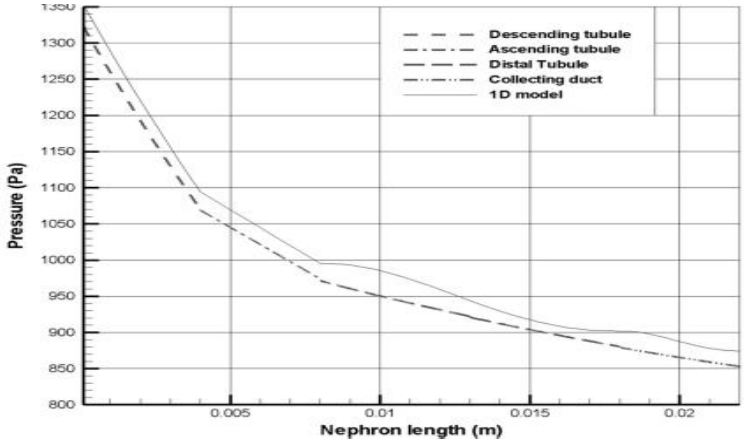

Figure 4. Pressure distribution along nephron from entrance of DHL to the end of CD in 3-D and 1-D model

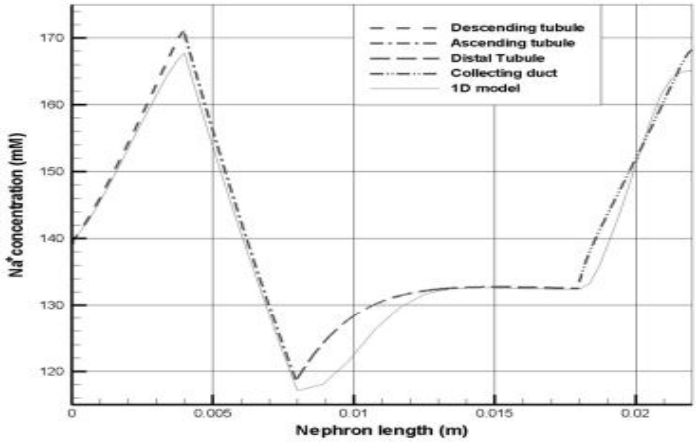

Figure 5. Na^+ concentration distribution along nephron from entrance of DHL to the end of CD in 3-D and 1-D model

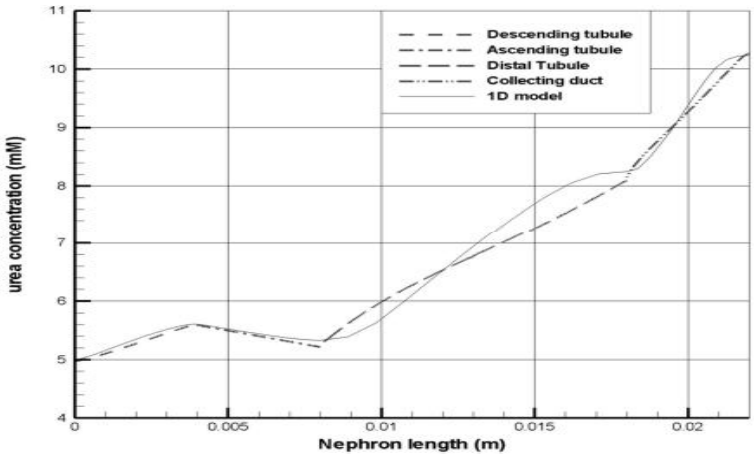

Figure 6. Urea concentration distribution along nephron from entrance of DHL to the end of CD in 3-D and 1-D model

3.1. Slip velocity

Since most of the biological fluid channels in human body are permeable and micron sized, the validity of no slip boundary condition on the channel wall and its influence on UCM should be checked [40] . In kidney, when the tubule's lumen exchanges fluid thorough its membrane, tangential velocity of fluid on the membrane surface practically is not zero. It should also be mentioned that investigating the slip effect at the membrane's surface on the concentrations, velocity and pressure distribution is just possible thorough 3-D numerical simulation of UCM. In this case, the tangential velocity on the membrane has been changed from $V_z = 0$ to $V_z = L_s\left(\frac{\partial V_r}{\partial z}\right)$ where L_s is the slip length and nondimensionlized by tubule's radius.

Comparison between Na^+ and urea concentration profiles of 3-D base-case model, no-slip boundary condition, and ones with dimensionless slip length equal to 0.05 and 0.1 showed no difference. Therefore, slip has no influence on species concentrations along nephron's length but as shown in Figure 7, the maximum velocity in the center of tubules decreases by increasing slip coefficient. Similarly, the pressure decreases as slip coefficient increases (Figure 8). Thus, the most significant effect of slip boundary condition is on the pressure distribution along nephron's length and subsequently upstream pressure, the glomerulus pressure.

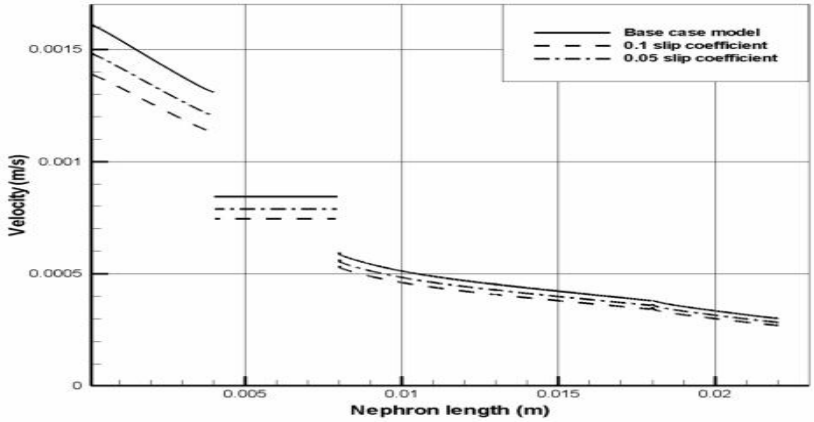

Figure 7. Effect of slip boundary condition on maximum velocity profiles along nephron

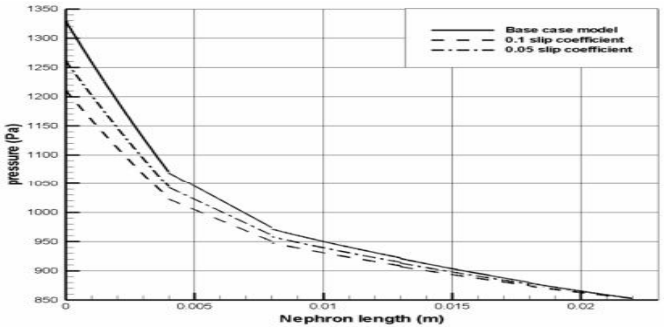

Figure 8. Effect of slip boundary condition on pressure profiles along nephron

3.2. Effect of diffusion coefficient of the OMI

The main objective of the current and subsequent sections is to answer the following questions: Is it possible to model and simplify the complexity of OMI, containing ascending and descending vessels, capillary beds, interstitial cells and spaces, with a homogenous intermediate interstitium by assigning effective value to diffusion coefficients and Darcy permeability? Besides, is it reliable enough to consider uniform concentration distributions over the OMI cross section, 1-D simulations, or mathematical modeling of renal should be done by 3-D simulation?

Primarily, in order to put more focus on investigating the effect of OMI diffusion coefficients on UCM, we have assumed OMI not to be porous, *i.e.* κ=1. Then, by assigning different values to interstitial solute permeability, we have been able to study its effect on radial species concentration gradient. One must note that diffusivities in intratubular regions have remained constant and equal to self-diffusion coefficients in dilute aqueous solution, 1.5×10^{-9} cm^2/s and 1.38×10^{-9} cm^2/s for Na^+ and urea, respectively [41].

Figure 9 demonstrates contours of urea and Na^+ concentration distributions at an arbitrary cross section, 3 mm from cortico-medullary boundary. As it has been expected, high values of solute permeability in the intermediate space practically results in uniform planar Na^+ and urea concentration distribution. On the other hand, as shown in Figures 9-A, B and C, by considerably reducing solute permeabilities, radial concentration contours emerge so we would be able to detect discernable planar osmotic gradient. It can be seen that in these cross sections, high and low concentration regions are situated next to each other. For instance, Na^+ concentration was distributed from 150 to 270 mM and urea concentration was distributed from 2.5 to 8 mM (Figure 9-C). In sum, these results show that species transport from tubules to the non-porous OMI is directly influenced by diffusion coefficient.

Figures 10-A and B display Na^+ and urea concentration profiles along nephron's length. It is shown that lower OMI solute diffusivities decrease the concentrating urine capability of a single nephron in this over simplified model structure, because urine at CD outlet would have lower osmolality. Furthermore, the pressure and velocity profiles along intratubular flux direction demonstrate that they can be directly affected by the changes in solute diffusivities (Figure 10-C and D). For instance, lower diffusion coefficients create the necessity for higher upstream static pressure. Moreover, higher maximum flow velocity at the end of DHL for lower OMI diffusivities means less water is reabsorbed from descending tubule. In other word, excessive radial confinement of tubules which can be imposed by lowering diffusion coefficient values can

practically block solutes and fluid interactions between tubules and consequently will result in reducing concentrating capability. On the other hand, cases with very high values of this parameter are unable to simulate the preferential interaction between tubules and the results are basically equivalent to 1-D simulations, uniform planar osmolality. In a word, the most important implication of this section is that this model parameter is perfectly capable of simulating tubular preferential interaction in which low diffusivities lead to more confinement between tubules and its higher values means no cross-sectional osmotic gradient. Moreover, it can be concluded that there exists an optimum value for this parameter to be consistency between simulation and experimental results. Unfortunately, the results from this over simplified structure are not able to clearly demonstrate the crucial significance of this parameter and its influence on system's optimal performance, but we have plan to find this optimum value by our complete 3-D simulation near future.

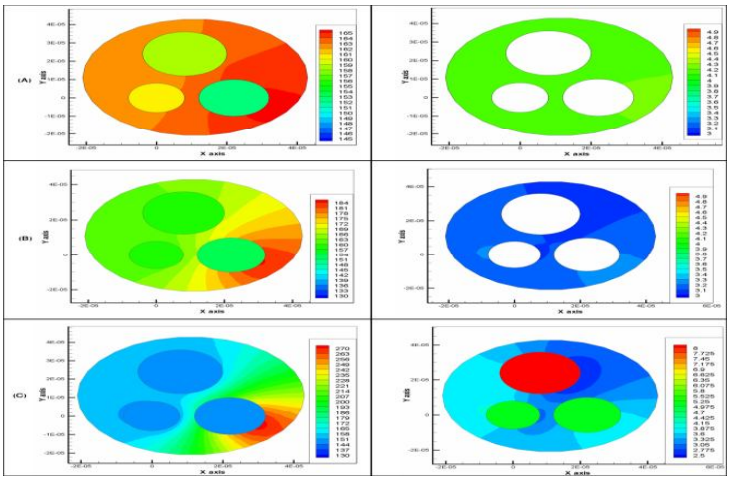

Figure 9. Na^+ and urea concentration contours respectively in left and right column at cross section 3 mm from cortico-medullary boundary for different diffusivity

$$: D = 5 \times 10^{-10} (m^2/s) \ , B: D = 5 \times 10^{-11} (m^2/s), C : D = 5 \times 10^{-12} (m^2/s)$$

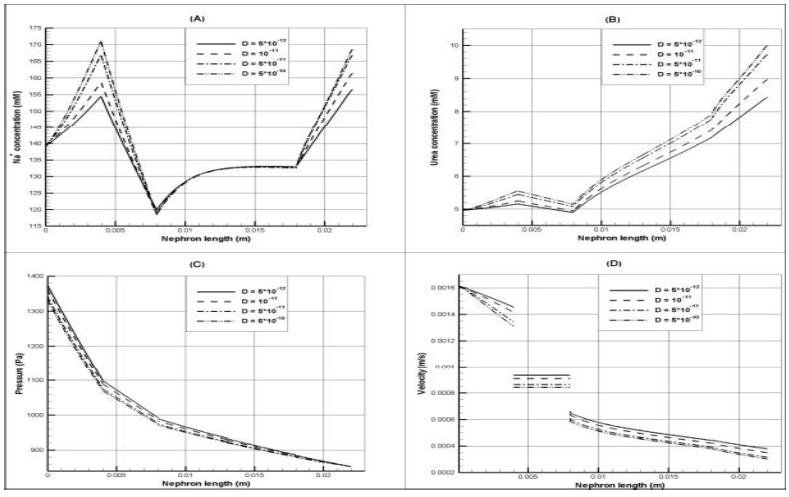

Figure 10. Effect of diffusion coefficient of the outer medullary interstitium on A: Na^+ concentration, B: urea concentration, C: pressure and D: maximum flow velocity distribution profiles along nephron

3.3. Effect of permeability of the OMI

Outer medulla consists of various compartments, *e.g.* tubules, ascending and descending vasa recta, interstitial cell, interstitial spaces and capillaries, making it very difficult to mathematically simulate interactions between these constituents. In order to simplify this complexity, outer medullary interstitium is considered to act as a porous intermediate vascular space. Therefore, by assigning proper values to Darcy permeability in x and y directions, we would be able to control the amount of radial fluid exchange and accordingly convective species transport between tubules. It should be noted that along z axis, due to central core assumption, Darcy permeability is assumed to be 1. It should be noted that in more complicated model structure with separate vasa recta, an appropriate Darcy permeability in cortico-meduallry direction should also be introduced. In this section, very low solute diffusivities have been used in order to amplify the influence of Darcy permeability on UCM. In addition, the influence of porosity has been just magnified to investigate its nature and give a rough estimate of its effect on UCM for more complex model structure.

In Figure 11-B, C and D, contours of axial velocity are demonstrated for different radial Darcy permeabilities varying from 10^{-15} to 10^{-19} m^2. Furthermore, for comparison purposes, the contours of the non-porous OMI are also shown in Figure 11-A. It is shown that radial porosity resistance, through creating high pressure gradient in the vicinity of each tubule, do not allow the reabsorbed fluid distributes radially and its upward flux toward cortex is confined to tubule's vicinity. Moreover, in order to provide a better insight into fluid exchange between tubules, radial velocity contours over the medulla cross section are also depicted in Figure 12-B, C and D, for different values of radial Darcy permeability. It could be perceived from Figures 11, 12 that due to extremely low interstitial fluid fluxes, axial and radial velocity contours practically do not change much for Darcy permeabilities below 10^{-15} m^2. Subsequently, the effect of porosity on planar species concentration gradients has also been studied for extremely porous, $\kappa = 10^{-19}$ m^2, as well as non-porous medullary interstitium (Figure 13-A, B).

Darcy permeability almost has seemingly had no influence on concentration contours but in what follows, it has been shown that it has affected concentration distributions along nephron's length (Figure 14). The differences between profiles of various OMI porosities arise from limiting radial convective fluid flow. Therefore, in descending tubule, reabsorption increases by lowering Darcy permeability which ultimately leads to slight rises in intratubular species concentrations. Moreover, it is apparent that because there is no water exchange across AHL membrane, its concentration profiles are not affected by porosity change. Since distal tubule interact with osmotically in equilibrium CI at a considerable length, Na^+ and urea concentrations converge to fixed values. Furthermore, in the collecting duct, the same process as DHL will also affect concentration profiles.

Another issue is the importance of hydraulic pressure differences versus osmotic pressure differences. It is generally considered that the latter are predominant in tubules, since the pressure exerted by a 1 mM concentration gradient is 19.4 mmHg and the results from this section also clearly supports this assumption. As shown in Figure 15, the most significant contribution of lowering Darcy permeability in OMI is drastically increasing local pressure in tubule's vicinity of course for very low diffusivities. Here, the diffusion coefficients are approximately 300 times lower than those in the tubules which may seem reasonable

because too much confinement have been imposed in order that porosity influence can be detectable.

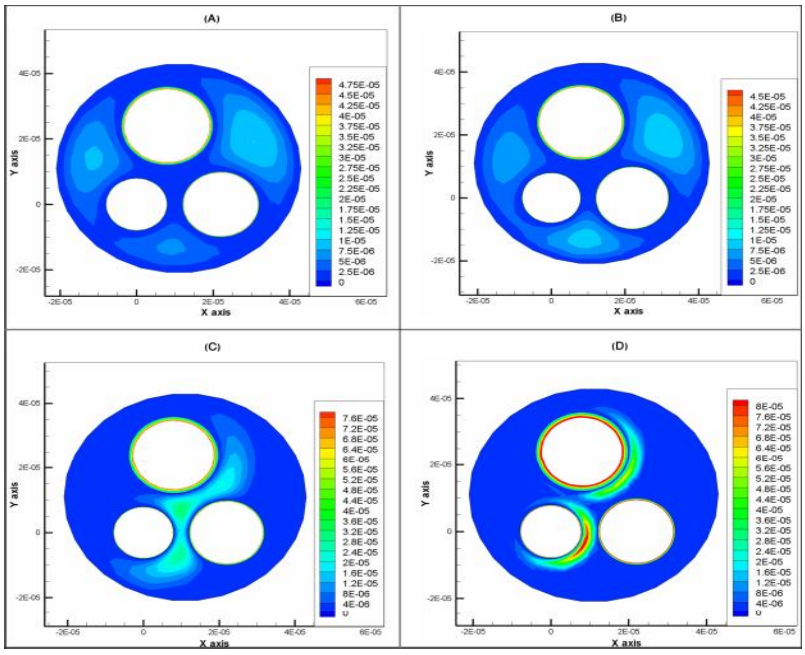

Figure 11. Axial velocity contour at cross section 3 mm from cortico-medullary boundary for OMI diffusivity$D = 5 \times 10^{-12} m^2/s$and different Darcy Permeability

$$A: k = 1m^2, B: k = 10^{-15} m^2, C: k = 11^{-17} m^2, D: k = 10^{-19} m^2$$

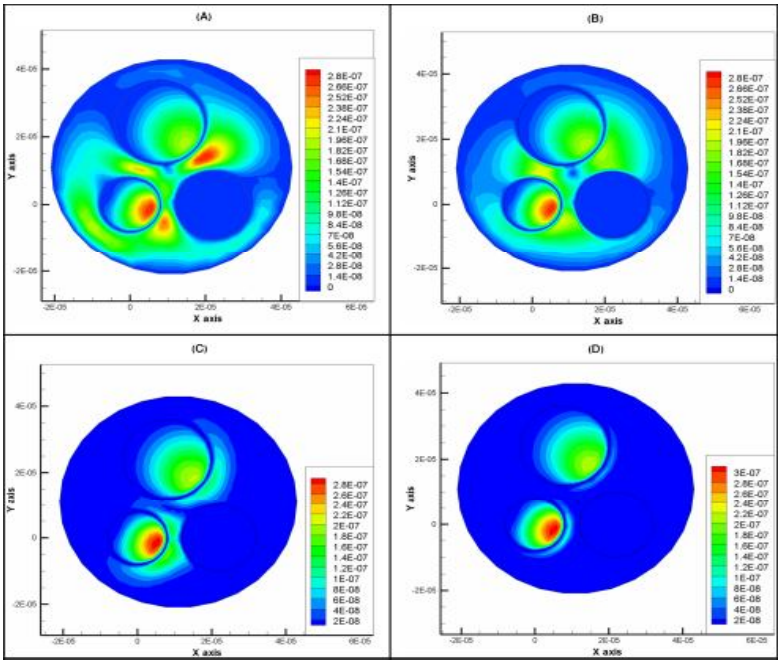

Figure 12. Radial velocity contour at cross section 3mm from cortico-medullary boundary for OMI diffusivit$D = 5 \times 10^{-12} m^2/s$y and different Darcy Permeability

$$A: k = 1m^2, B: k = 10^{-15} m^2, C: k = 11^{-17} m^2, D: k = 10^{-19} m^2$$

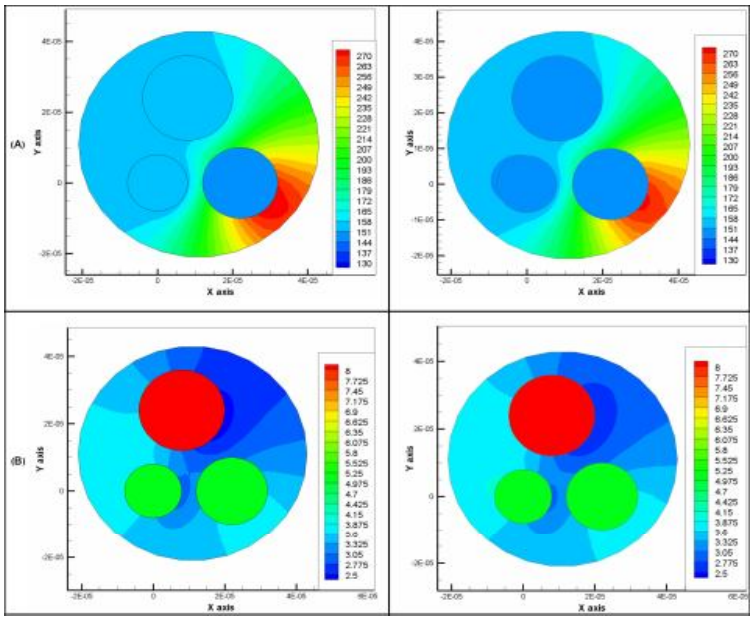

Figure 13. Na^+ and urea concentration contours respectively in row A and B at cross section 3 mm from cortico-medullary boundary for OMI diffusivity $D = 5 \times 10^{-12} m^2/s$ and different Darcy Permeability;

$$Left: k = 1m^2 \, , Right: k = 10^{-19} m^2$$

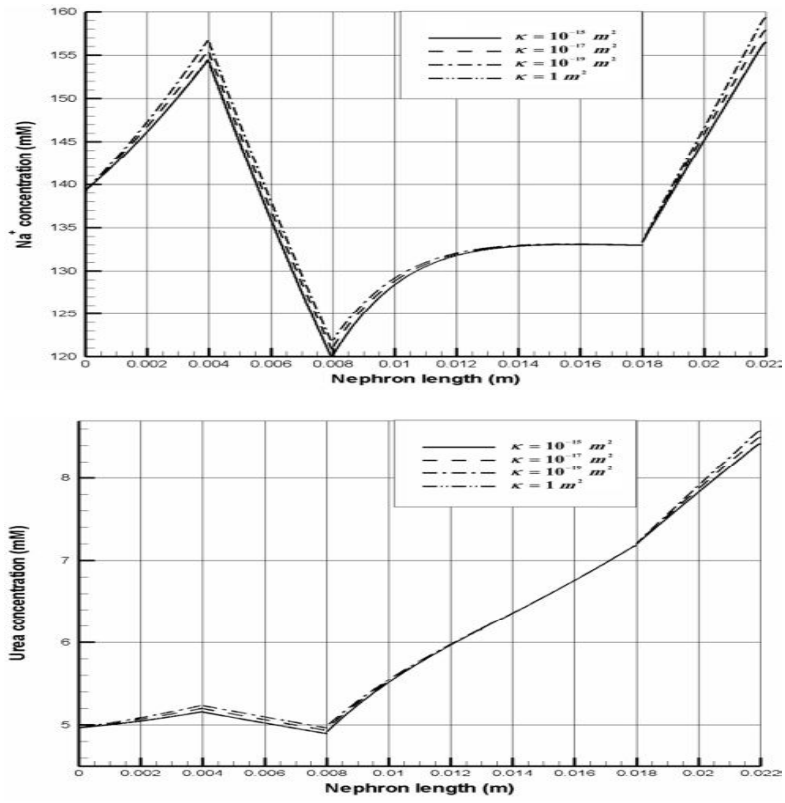

Figure 14. Effect of Darcy permeability on Na^+ and urea concentrations distribution profiles along Nephron for OMI diffusivity$D = 5 \times 10^{-12} m^2/s$

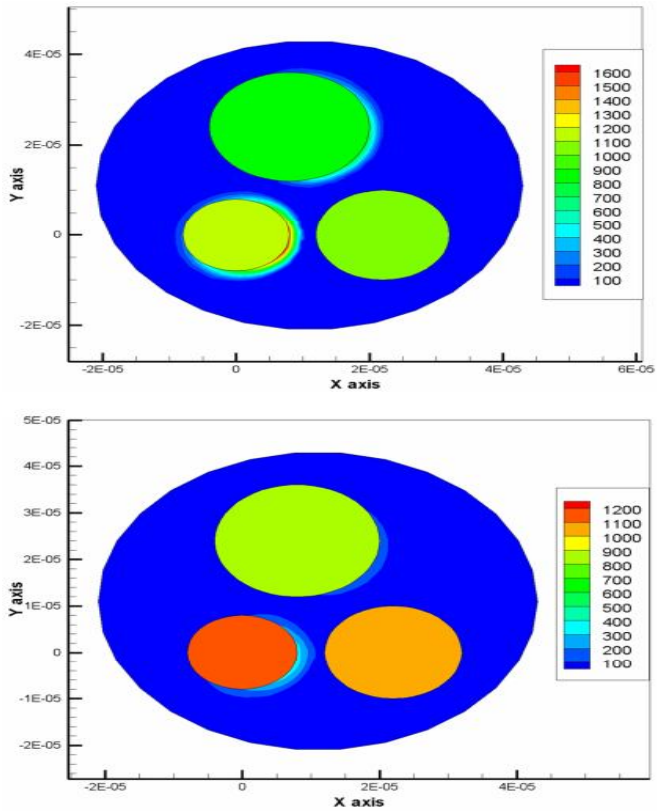

Figure 15. Pressure contour at cross section 3mm from cortico-medullary boundary for OMI diffusivity$D = 5 \times 10^{-12} m^2/s$and different Darcy Permeability; up: $10^{-19} m^2$, $down$: $k = 10^{-18} m^2$

4. Conclusions

In order to study the effects of outer medulla's structural properties on the UCM, a simple 3-D model was described in this paper. Darcy permeability and solute's diffusivity of the intermediate media are two important properties which were chosen to investigate their influence on the UCM. Besides, we also studied the effects of slip boundary condition on tubules' membrane because of its major role in mass transfer. The most distinguishable advantage of our 3-D approach is that this behavior could be modeled by having control over solute's diffusion and Darcy permeability coefficients of OMI. This 3-D modeling was just a framework to reach a converged numerical solution for the momentum and species transport equations along with their coupled membrane fluxes using our native code. Due to this reason, the model structure and their membrane specification were assumed to be as simple as possible. Therefore, the results from this simple 3-D simulation were not that accurate to be compared with experimental data. But, our 3-D approach was evaluated against its equivalent one-dimensional model in the first part of our data analysis.

Although there were some simplifying assumptions in our model, we could simulate preferential interactions and more importantly the radial concentration gradients by assigning specific values to physical properties like Darcy and solute permeability. On the whole, we believe that this approach will play an important role in obtaining a deeper understanding about the effect of tubular and vascular 3-D architecture and their interactions in UCM.

Nomenclature

i	Tubule or medulla superscript	$V^i_{max,k}$	Maximum transport rate, $\frac{mol}{m^2 s}$
k	Solute subscript	$K^i_{M,k}$	Michaelis constant, $\frac{mol}{m^3}$
J^i_v	Transtubular water flux, $\frac{m}{s}$	D^i_k	Diffusion coefficient, $\frac{m^2}{s}$
J^i_k	Transtubular solute flux, $\frac{mol}{m^2 s}$	μ	Fluid viscosity, $\frac{kg}{m.s}$
P^i	Pressure, ^{pa}	ρ	Fluid density, $\frac{kg}{m^3}$
F^i_v	Water flow rate, $\frac{m^3}{s}$	R_g	Universal gas constant, $\frac{J}{mol.K}$
F^i_k	Solute flow rate, $\frac{mol}{m^3 s}$	T	Absolute temperature, K
C^i_k	Solute concentration, $\frac{mol}{m^3}$	r^i	Radius, m
h^i_v	Hydraulic permeability, $\frac{m}{Pa.s}$	L_i	Length , m
h^i_k	Solute permeability, $\frac{m}{s}$	V	Velocity vector, $\frac{m}{s}$
ϕ^i_k	Reflection coefficient	κ	Porous media permeability, m^2
$\phi_{osm,k}$	Osmolality coefficient	L_s	Slip length, m

Abbreviations

AHL= Ascending Henle's loop
AVRs= Ascending vasa recta
CC= Central core
CD= Collecting duct
CI= Cortical interstitium
DHL= Descending Henle's loop
DT= Distal tubule
DVRs= Descending vasa recta
OM= Outer medulla
OMI= Outer medullary interstitium
UCM= Urine concentration mechanism

Conflict of interest

The authors declare that there is no conflict of interest.

Consent for publications

All authors read and approved the final manuscript for publication.

Availability of data and material

All authors declare that they embedded all data in the manuscript.

Authors' contributions

S.S., M.H.B. and S.S.L. did the simulation work, S.S. and M.S wrote the main manuscript and analyzed the simulation results, M.S.S, M.S. and B.F. guided the research and reviewed the manuscript, H.H. revised the manuscript.

Ethics approval and consent to participate

The authors declared that they do not use human or animals in their research.

Funding

There is no funding.

5. References

1. Qian, Q. (2018). Salt, water and nephron: Mechanisms of action and link to hypertension and chronic kidney disease. *Nephrology*, 23:44-49.
2. Layton, AT. (2017). A new microscope for the kidney: mathematics. *Am. J. Physiol. Renal Physiol.,* 312(4):F671-F672.
3. Layton, HE. (2002). Mathematical models of the mammalian urine concentrating mechanism. *Ima Volumes In Mathematics And Its Applications*, 129(1):233-272.
4. Sohrabi, S, Saidi, MS, Saadatmand, M, Banazadeh, MH, Firoozabadi, B. (2014). Three-dimensional simulation

of urine concentrating mechanism in a functional unit of rat outer medulla. I. Model structure and base case results. *Mathemat. Biosci.*, 258:44-56.
5. Burg, M, Green, N. (1973). Function of the thick ascending limb of Henle's loop. *Am. J. Physiol. Legacy Content*, 224(3):659-668.
6. Rocha, AS, Kokko, JP. (1973). Sodium chloride and water transport in the medullary thick ascending limb of Henle. Evidence for active chloride transport. *J. Clin. Investigat.*, 52(3):612-623.
7. Chou, C, Knepper, M. (1992). In vitro perfusion of chinchilla thin limb segments: segmentation and osmotic water permeability. *Am. J. Physiol. Renal Physiol.*, 263(3):F417-F426.
8. Imai, M, Kokko, JP. (1974). Sodium chloride, urea, and water transport in the thin ascending limb of Henle. Generation of osmotic gradients by passive diffusion of solutes. *J. Clin. Investigat.*, 53(2):393-402.
9. Marsh D, Azen, SP. (1975). Mechanism of NaCl reabsorption by hamster thin ascending limbs of Henle's loop. *Am. J. Physiol. Legacy Content*, 228(1):71-79.
10. Yool, AJ, Brokl, OH, Pannabecker, TL, Dantzler, WH, Stamer, WD. (2002). Tetraethylammonium block of water flux in Aquaporin-1 channels expressed in kidney thin limbs of Henle's loop and a kidney-derived cell line. *BMC Physiol.*, 2(1): 4.
11. Stephenson, JL. (1972). Concentration of urine in a central core model of the renal counterflow system. *Kidney Int.,* 2(2):85-94.
12. Kokko, J, Rector Jr, F. (1972). Countercurrent multiplication system without active transport in inner medulla. *Kidney Internat.*, 2(4):214-223.
13. Wang, X, Thomas, SR, Wexler, AS. (1998). Outer medullary anatomy and the urine concentrating mechanism. *Am. J. Physiol. Renal Physiol.,* 274(2):F413-F424.
14. Wexler, AS, Kalaba, RE, Marsh, DJ. (1991). Three-dimensional anatomy and renal concentrating mechanism. I. Modeling results. *Am. J. Physiol. Renal Physiol.*, 260(3):F368-F383.
15. Pannabecker, TL, Dantzler, WH, Layton, HE, Layton, AT. (2008). Role of three-dimensional architecture in the urine concentrating mechanism of the rat renal inner medulla. *Am. J. Physiol. Renal Physiol.,* 295(5):F1271-F1285.
16. Zhai, XY, Thomsen, JS, Birn, H, Kristoffersen, IB, Andreasen, A, Christensen, E. (2006). Three-dimensional reconstruction of the mouse nephron. *J. Am. Soc. Nephrol.*, 17(1):77-88.
17. Layton, A.T, Layton, H.E. (2005). A region-based mathematical model of the urine concentrating mechanism in the rat outer medulla. I. Formulation and base-case results. *Am. J. Physiol. Renal Physiol.*, 289(6):F1346-F1366.
18. Layton, AT, Pannabecker, TL, Dantzler, WH, Layton, HE. (2010). Functional implications of the three-dimensional architecture of the rat renal inner medulla. *Am. J. Physiol. Renal Physiol.*, 298(4):F973-F987.
19. Bentley, M, Jorgensen, S, Lerman, L, Ritman, E, Romero, J. (2007). Visualization of three-dimensional nephron structure with microcomputed tomography. *ANAT. REC*, 290(3): 277-283.
20. Kriz, W, Kaissling, B. (1992). Structural organization of the mammalian kidney. *Kidney Physiol. Pathophysiol.*, 3:587-654.
21. Pannabecker, TL, Dantzler, WH. (2004). Three-dimensional lateral and vertical relationships of inner medullary loops of Henle and collecting ducts. *Am. J. Physiol. Renal Physiol.*, 287(4):F767-F774.

22. Layton, AT, Layton, HE. (2003). A region-based model framework for the rat urine concentrating mechanism. *Bull. Mathemat. Boil.*, 65(5):859-901.
23. Layton, AT, Vallon, V. (2018). Renal tubular solute transport and oxygen consumption: insights from computational models. *Curr. Opin. Nephrol. Hypertens.*, 27(5):384-389.
24. Layton, AT. (2017). Tracking the Distribution of a Solute Bolus in the Rat Kidney Women in Mathematical Biology (pp. 115-136): *Springer*.
25. Chen, Y, Fry, B, Layton, A. (2017). Modeling glucose metabolism and lactate production in the kidney. *Mathemat. Biosci.,* 289:116-129.
26. Sgouralis, I, Layton, AT. (2015). Mathematical modeling of renal hemodynamics in physiology and pathophysiology. *Mathemat. Biosci.*, 264:8-20.
27. Layton, AT, Laghmani, K, Vallon, V, Edwards, A. (2016). Solute transport and oxygen consumption along the nephrons: effects of Na+ transport inhibitors. *Am. J. Physiol. Renal Physiol.*, 311(6):F1217-F1229.
28. Sgouralis, I, Layton, AT. (2017). Modeling blood flow and oxygenation in a diabetic rat kidney Women in Mathematical Biology (pp. 101-113): *Springer*.
29. Wexler, AS, Marsh, DJ. (1991). Numerical methods for three-dimensional models of the urine concentrating mechanism. *Appl. Mathemat. Computat.,* 45(2):219-240.
30. Sohrabi S, Saidi M S, Saadatmand M, Banazadeh M H, Firoozabadi B. (2014). Three-dimensional simulation of urine concentrating mechanism in a functional unit of rat outer medulla. I. Model structure and base case results. *Mathemat. Biosci.*, 258:44-56.
31. Kriz, W., Kaissling, B. (2000). Structural organization of the mammalian kidney *The kidney physiology and Pathophysiology (3d ed). Philadelphia: Lippincott Williams Wilkins*: 588-654
32. Layton H E. (2002). Mathematical Models of the Mammalian Urine Concentrating Mechanism. *Membrane Transport Renal Physiol.,* 129.
33. Stephenson, J. L., Zhang, Y., Eftekhari, A., Tewarson, R. (1987). Electrolyte transport in a central core model of the renal medulla. *Am. J. Physiol.*, 253(5 Pt 2):F982-997.
34. Mirbagheri, S.A, Saidi, M.S, Sohrabi, S, Firoozabadi, B, Banazadeh, M.H. (2016). Effects of hypertension on Intima-Media Thickness (IMT); application to a human carotid artery. *Sci. Iranica*, 23(4):1731-1740.
35. Kedem, O, Katchalsky, A. (1963). Permeability of composite membranes. Part 1. Electric current, volume flow and flow of solute through membranes. *Transact. Faraday Soc.,* 59:1918-1930.
36. Sani, M, Saeidi, MS. (2010). Rayan: A polyhedral grid co-located incompressible finite volume solver (part I: basic design features).
37. Sani, M, Saidi, MS. (2009). A set of particle locating algorithms not requiring face belonging to cell connectivity data. *J. Computat. Phys.,* 228(19):7357-7367.
38. Sani, M, Saidi, MS. (2010). A lagged implicit segregated data reconstruction procedure to treat open boundaries. *J. Computat. Phys*, 229(14):5418-5431.
39. Lide, D.R. (2001). CRC Handbook of Chemistry and Physics. *82th edn. Cleveland, OH: CRC*.
40. Sani, M, Saidi, MS. (2010). A lagged implicit segregated data reconstruction procedure to treat open boundaries. *J. Computat. Phys.,* 229(14):5418-5431.

41. Sohrabi, S, Nemati Mehr, SM, Falsafi, P. (2013). A Novel Approach for Compensating the Significance of Tubule's Architecture in Urine Concentrating Mechanism of Renal Medulla. Paper presented at the *ASME 2013 International Mechanical Engineering Congress and Exposition*.

How to cite this article: Maryam Saadatmand, Mohammad Said Saidi, Salman Sohrabi, Mohamad Hossein Banazadeh, Saeed Sadeghi Lafmejani, Hamid Hamed, Bahar Firoozabadi, A 3-Dimentional Framework for Studying the Effects of Structural and Physical Properties of the Renal Outer Medulla on Urine Concentrating Mechanism. *International Journal of Advanced Biological and Biomedical Research*, 2021, 9(1), 28-47. Link: http://www.ijabbr.com/article_44618.html